

# A STUDY OF THE DIELECTRIC AND ELECTRICAL PROPERTIES OF THE MATRIX COMPOSITE [Ba<sub>2</sub>CoNbO<sub>6</sub> (BCNO)<sub>1-x</sub> - CaTiO<sub>3</sub>(CTO)<sub>x</sub>]

J. E. V. de Morais<sup>1,2</sup>; A. J. N. de Castro<sup>1,2</sup>; J. C. Sales<sup>1,2,5</sup>; V. L. Bessa<sup>1,2</sup>; R. G. M. Oliveira<sup>1,2</sup>; W. V. S. Reis<sup>2,3</sup>; F. F. do Carmo<sup>2</sup>; J. P. C. do Nascimento<sup>2</sup>; M. A. S. Silva<sup>2</sup>; A. S. B. Sombra<sup>1,2,4</sup>

<sup>1</sup>Telecommunication Engineering Department, Federal University of Ceara (UFC) P.O. Box 6007, Fortaleza, Ceará 60755-640, Brazil

<sup>2</sup>Physics Department - Telecommunication, Science and Engineering of Materials Laboratory (LOCEM), Federal University of Ceara (UFC), P.O. Box 6030, Fortaleza, Ceará. 60455-760, Brazil, 55(85)33669334 / FAX 33669332. <http://www.locem.ufc.br>

<sup>3</sup>Federal Institute of Ceará, Campus Fortaleza/IFCE, ZIP CODE 63400-000, Fortaleza, Ceará, Brazil.

<sup>4</sup>Laboratory of Communication and Security Networks (LARCES), State University of Ceará, Itaperi Campus, Fortaleza, Ceará, Brazil.

<sup>5</sup>State University Vale do Acaraú - Department of Civil Engineering.

## Abstract

In this work, composites based on the ceramic matrix Ba<sub>2</sub>CoNbO<sub>6</sub> (BCNO)<sub>1-x</sub> - CaTiO<sub>3</sub>(CTO)<sub>x</sub> were fabricated using the solid-state reaction method. X-ray diffraction and scanning electron microscopy were used for structural and morphological characterization of the material. The dielectric properties of the composites in the microwave and radio frequency ranges were analysed, as well as the temperature dependence, using the Hakki-Coleman and Silva-Fernandes-Sombra methods for microwave analysis and complex impedance spectroscopy for radio frequency analysis. A cylindrical resonator was fabricated from a mixture of Ba<sub>2</sub>CoNbO<sub>6</sub> and CTO using 0, 5, 12, 20 and 37 wt. % of CTO and sintering of these composites. CTO insertion improved the thermal stability of the material and showed interesting results in the radio and microwave frequency ranges. Tests of the samples operating as an antenna were performed and showed that all samples were operating in the range of 3–5 GHz.

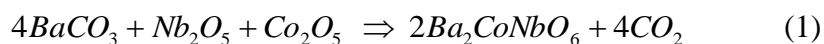
Keyword: BCNO, CTO, dielectric properties, microwave, thermal stability, DRA.

## Introduction

The main characteristics of ceramic materials are good mechanical resistance, thermal resistance and chemical stability. Because they have these characteristics, they are attractive in a wide range of industries that can apply them in the manufacture of new products and/or insert them in industrial processes [1,2]. The development of new materials that can be applied in the telecommunications, aerospace, military and medical industries has grown greatly in recent years. This growth has happened due to the study of advanced ceramic materials [3] in conjunction with the study of families of structures, such as perovskite, rutile, spinels and others, that have important electrical and dielectric properties in the radio-frequency and microwave ranges [4,5]. Some of these properties are high permittivity and low dielectric loss, which can be applied to the building of high-quality electronic materials and high-frequency circuits, both with low manufacturing costs [4,6]. Ba<sub>2</sub>CoNbO<sub>6</sub> (BCNO) is a ceramic material consisting of oxides with a perovskite structure oxides, cubic symmetry [7] and a high-temperature coefficient of resonant frequency [8]. In the literature, BCNO presents some important properties such as a low-temperature phase transition [9], a large dielectric constant and interesting properties in the radio frequency band [10,11]. CaTiO<sub>3</sub> (CTO) has attracted researchers' attention because of its high dielectric permittivity in the microwave range, low dielectric loss and a very high resonance temperature coefficient ( $\tau_f$ ) [2]. In this work, the properties of BCNO and CTO were combined. The combination of BCNO and CTO can exhibit thermal stability ( $\tau_f$ ) close to zero since the materials have opposite signs for  $\tau_f$ . For this reason, cylindrical resonators were prepared to study the properties of the composites in the radio and microwave frequency ranges at room temperature. X-ray diffraction (XRD) was used to analyse the crystallographic phases, while dielectric and electric properties and thermal stability of the mixture of BCNO and CTO were analysed by complex impedance spectroscopy (CIS), the Hakki-Coleman method [12] and the Silva-Fernandes-Sombra method (SFS) [13]. The composites were constructed for evaluation as Dielectric Resonator Antenna (DRA) and simulated using HFSS® software (high-frequency structural simulator) and the parameters analysed were the coefficient of reflection (S<sub>11</sub>), gain, Smith chart and radiation pattern.

## Experimental Procedure

BCNO was prepared using the conventional solid-phase reaction method. A stoichiometric blend of high purity oxides (BaCO<sub>3</sub> (99%, Vetec), Nb<sub>2</sub>O<sub>5</sub> (99%, Aldrich) and Co<sub>2</sub>O<sub>3</sub> (97%, Vetec)) was used and mixed in a mortar. The blends were milled for 6h in a ball mill with polyacetal pans and zirconia balls, then placed in the oven for 6h at 850°C. The material was pressed at 200 MPa in a uniaxial press and sintered in a furnace at 1000°C for 5 h. Both heating and cooling were maintained at a 5°C per minute rate, forming the phase shown in Eq.1.

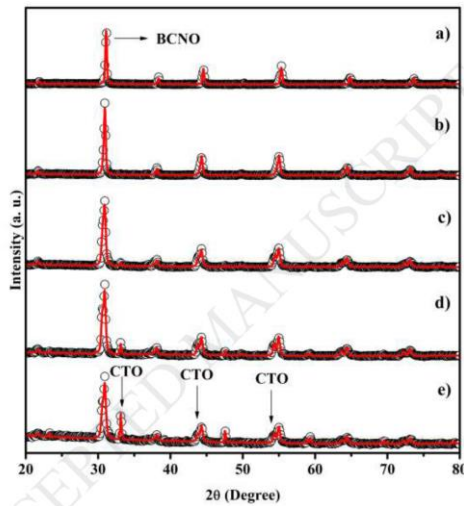


The powders obtained in this process were examined using the XRD technique with  $\text{K}\alpha$ - Cu radiation ( $\lambda = 0.15406 \text{ \AA}$ ) in a range of  $20\text{--}80^\circ$  at a rate of  $0.5^\circ$  per minute to identify the  $\text{Ba}_2\text{CoNbO}_6$  phase. The samples were prepared with the addition of 0, 5, 12, 20 and 37%wt CTO and are represented as BCNO00, BCNO05, BCNO12, BCNO20 and BCNO37, respectively. Dielectric properties such as dielectric loss and permittivity were obtained in microwave range using the Hakki-Coleman method. Also in microwave range, the temperature coefficient of the resonant frequency,  $\tau_f$ , was measured using the SFS method and an Agilent AN5230A network analyser. The antenna measurements were performed using the reflection coefficient, an Agilent N5230A network analyser and HFSS software. In order to perform the electrical measurements at radio frequencies, the pellets were painted with silver paste on both sides and then heated at  $600^\circ\text{C}$  for 1 h to remove its polymeric components. The parameters were measured as a function of frequency in the range of 1Hz to 10MHz at room temperature using an impedance analyser (Solartron 1260).

## Results

BCNO synthesis was analysed by XRD and the phase confirmation was performed using the Rietveld refinement [14] in which all the peaks that are in the experimental measurements were compared with the diffraction peaks of the ICSD 91086 standard, which shows cubic symmetry and space group  $\text{pm}3\text{m}$  [8]. The Rietveld refinement was performed, and the parameters revealed good agreement with the BCNO ICSD standard, where  $\text{RWP} = 9.25\%$ ,  $S = 1.35$ ,  $\text{RBragg} = 4.20$ , and the monocrystal density was  $6.42 \text{ g.cm}^{-3}$ . These values represent a good refinement because the lattice parameters are close to the standard ICSD 91086. The diffraction analysis of the blends is shown in Fig. 1 and Table 1.

Figure1: X-ray diffraction patterns BCNO and BCNO-CTO.



The diffractogram shows the evolution of BCNO and CTO peaks with increasing CTO addition, Fig. 1a–e. The CTO peaks appear more intensely with increasing CTO addition and there is no extra important phase found during refinement.

Table1: Parameters obtained from Rietveld refinement of the BCNO-CTO

Sample	REXP(%)	RP(%)	Rwp(%)	S
BCNO	6,84	7,13	9,25	1,35
BCNO05	2,78	3,45	4,48	1,61
BCNO12	2,85	4,02	5,41	1,89
BCNO20	2,89	4,19	9,61	1,93
BCNO37	3,23	4,80	5,93	1,83

The validity of the sintering process was analysed using pycnometry, as shown in Table 2 and the SEM images in Fig. 2. Sample density values decrease with CTO insertion, which is expected since CTO has a lower density than BCNO [2, 15].

Table 2: Dielectric properties of BCNO and BCNO-CTO in the microwave range

Sample	Radius (mm)	Height (mm)	Diâmeter	$\sigma_E$ (g.cm <sup>-1</sup> )	$\epsilon'_{Ex}$ <sub>p</sub>	Tan ( $\delta_{Exp}$ )
BCNO	7.04	5.75	14.08	4.47	15.7	$2.78 \cdot 10^{-2}$
BCNO05	7.21	7.36	14.42	3.88	17.4	$3.54 \cdot 10^{-2}$
BCNO12	7.42	7.92	14.83	3.56	18.8	$5.20 \cdot 10^{-2}$
BCNO20	7.45	8.46	14.91	3.33	18.4	$4.11 \cdot 10^{-2}$
BCNO37	7.49	7.03	14.97	3.03	18.7	$4.28 \cdot 10^{-2}$

Figure 2: SEM images of BCNO and composites (a) BCNO, (b) BCNO05, (c) BCNO12, (d) BCNO20, (e) BCNO37.

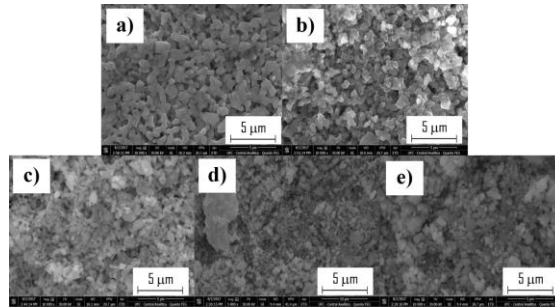


Table 3 shows the permittivity as a function of frequency at room temperature in the frequency range from 1Hz to 10MHz. The dielectric permittivity of BCNO with the addition of CTO decreases with increasing frequency, see Fig 3a, indicating either a relaxation phenomenon where while the rotated dipoles do not follow the electric field at high frequencies or an electrode effect [16].

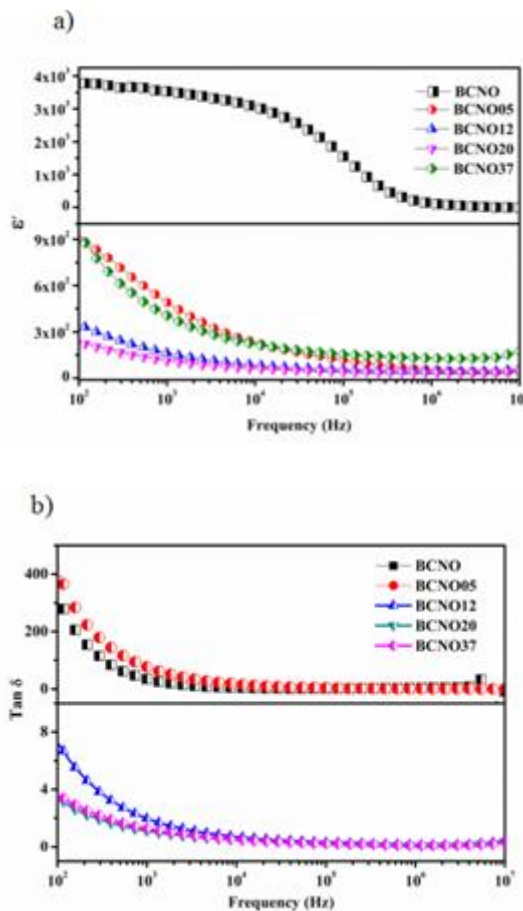
Table 3: The dielectric properties of ceramics BCNO, BCNO05, BCNO12, BCNO20 and BCNO37

Sample	100 HZ		10kHz		100kHz	
	$\epsilon'$	Tan $\delta$	$\epsilon'$	Tan $\delta$	$\epsilon'$	Tan $\delta$
BCNO	3780	326	3060	4.19	1550	1.56
BCNO05	896	419	231	16.8	119	3.67
BCNO12	351	7.25	85.5	0.70	55.4	0.30
BCNO20	236	3.41	63.3	0.48	44	0.23
BCNO37	936	3.65	221	0.51	155	0.23

At low frequencies, the dielectric losses are higher for BCNO and BCNO05, what happens because BCNO present, higher loss compared to CTO [17] and, in these samples, the BCNO molar fraction is much larger than the CTO molar fraction in another samples. Thus, this explains the proximities of the curves in Fig.3a and Fig.3b. For samples BCNO12, BCNO20 and BCNO37, the molar fraction of CTO is much higher than the molar fraction of BCNO.

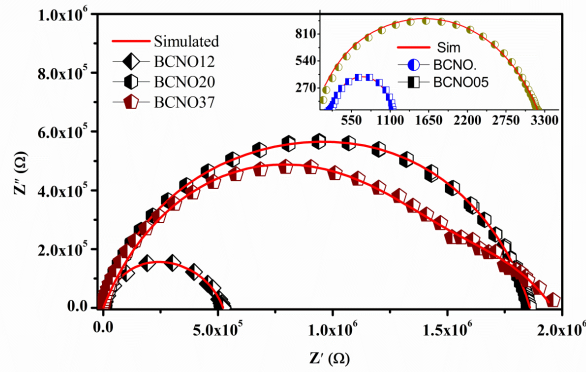
The dielectric losses follow a downward trend due to the CTO, as seen in Fig. 3b. The highest permittivity value occurs for the BCNO at 100 Hz and the lowest dielectric loss occurs for the BCNO37 sample at 1 MHz, see Table 3.

Figure 3: Relative dielectric permittivity and (b) loss tangent as a function of frequency for BCNO-CTO.



The impedance diagram, Nyquist diagram, of the BCNO with added CTO at room temperature is shown in Fig 4.

Figure 4: Variation of real part ( $Z'$ ) versus the imaginary part ( $Z''$ ) of the complex impedance of BCNO-CTO at room temperature.



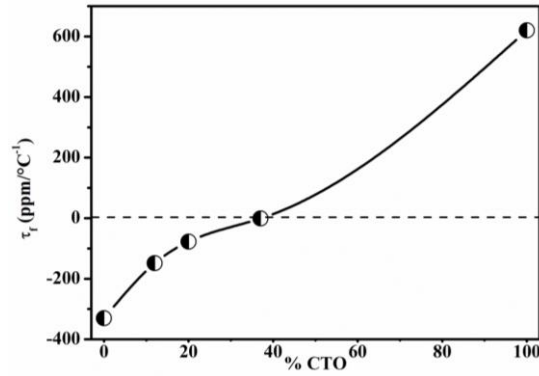
This diagram is typical of ceramic materials and for a good fit of the circuit we use two RC circuits; although the results only present a semicircle, the circuits are associated with the grain and the grain boundary of the ceramics. We use the constant phase element (CPE) instead of the capacitance because CPE is a generalized element. Several factors can contribute to CPE, one of the main factors being irregularities on the surface of the electrodes [18]. The addition of CTO considerably increased the impedance of BCNO, as seen in Table 4, which shows increasing values for resistors R1 and R2.

Table 4: Equivalent circuit fitting parameters for BCNO-CTO.

Sample	Grain			Grain Boundary		
	R <sub>1</sub>	P <sub>1</sub>	n <sub>1</sub>	R <sub>2</sub>	P <sub>2</sub>	n <sub>2</sub>
BCNO	3.01·10 <sup>2</sup>	4.14·10 <sup>-6</sup>	0.40	8.40·10 <sup>2</sup>	1.45·10 <sup>-8</sup>	0.92
BCNO05	3.00·10 <sup>3</sup>	1.18·10 <sup>-8</sup>	0.69	2.25·10 <sup>2</sup>	4.19·10 <sup>-10</sup>	1.00
BCNO12	2.72·10 <sup>5</sup>	1.11·10 <sup>-8</sup>	0.70	2.51·10 <sup>5</sup>	1.51·10 <sup>-9</sup>	0.80
BCNO20	1.22·10 <sup>6</sup>	3.15·10 <sup>-9</sup>	0.76	6.43·10 <sup>5</sup>	1.24·10 <sup>-9</sup>	0.79
BCNO37	1.35·10 <sup>6</sup>	1.76·10 <sup>-9</sup>	0.73	6.08·10 <sup>5</sup>	1.28·10 <sup>-7</sup>	0.55

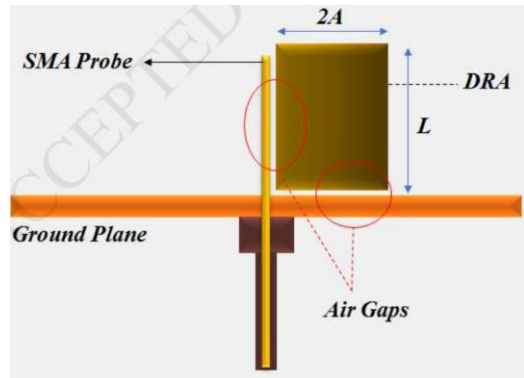
The values of n for the grain are in the range of 0.4–0.7, indicating that CPE is related to diffusion and deviations relative to Fick's second law. For the grain boundary, n, CPE is close to 1 for BCNO and BCNO05, indicating that the CPE represented is much more capacitive, whereas for samples BCNO12, BCNO20 and BCNO37, it decreases to 0.545 [18]. The dielectric properties of ceramic cylinders in the microwave range were measured by the Hakki-Coleman technique. All samples presented radius/height ratios close to one, which is required by the technique. The compounds did not show the expected increase in the dielectric permittivity and dielectric loss with the increase of the CTO concentration [19], as seen in Table 2. This can be explained by the sintering temperature, which in the literature can be higher than 1200°C [20], chosen for the material. The temperature coefficient of the resonant frequency was measured in all samples by the SFS method. The measurements of τf for BCNO showed that the negative values become positive with the addition of CTO, thus improving the thermal stability of the dielectric properties of the studied ceramic, as seen in Fig. 5.

Figure 5: Temperature coefficient of the resonant frequency of BCNO-CTO composites.



The improvement in the thermal stability with CTO addition occurred because CTO ( $\tau_f = 625 \text{ ppm} \cdot \text{C}^{-1}$ ) [13] presents opposite  $\tau_f$  values compared to BCNO and, in the sample with 37%wt of CTO, it presented better thermo-stability, according to Table 2, from this CTO concentration the  $\tau_f$  values increases for  $\tau_f$  positive values due to the CTO properties. BCNO was tested as a DRA. Figure 6 shows the experimental setup for the antenna tests, where **A** is the radius and **L** is the height of the DRA.

Figure 6: Design of dielectric resonator antenna measurement.



The antenna feed is lateral, considering that the dominant mode is the  $HE_{11\delta}$ . Eq. 2 shows the frequency of the fundamental mode.

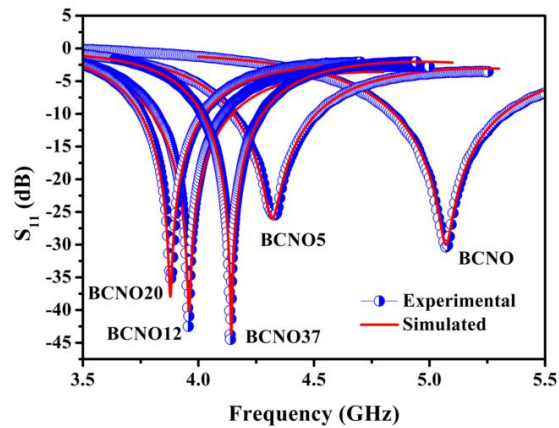
$$f_{HE_{11\delta}} = \frac{2.735c\epsilon_r^{-4.036}}{2\pi A} \left[ 0.543 + 0.589 \frac{A}{2L} - 0.050 \left( \frac{A}{2L} \right)^2 \right] \quad (2)$$

$$Q_{HE_{11\delta}} = 0.013\epsilon_r^{1.202} \left[ 2.135 \left( \frac{A}{2L} \right) + 228.043 \left( \frac{A}{2L} \right) e^{-2.046 \left( \frac{A}{2L} \right) 0.111 \left( \frac{A}{2L} \right)^2} \right] \quad (3)$$

It can be seen that BCNO functions as a DRA as long as the reflection coefficient (S11) is below -10 dB, showing that there is an acceptable minimum reflection. Fig. 7 shows that all samples function as

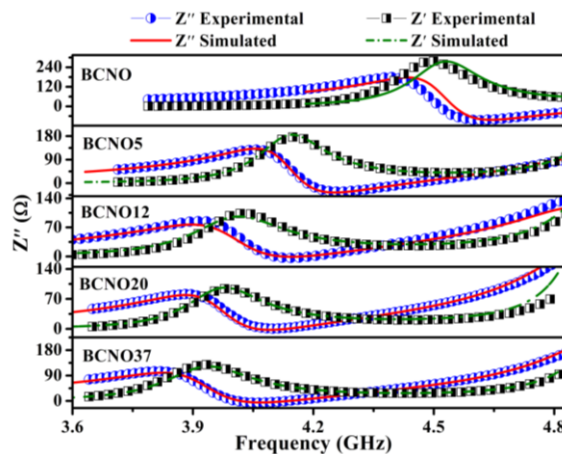
antenna. We noticed that there is a narrowing of the DRA's bandwidth of with the addition of CTO, which can be explained by Eq. 3, where the quality factor is a function of the material geometry and the electric constant [21].

Figure 7: Experimental reflection coefficient measurements for BCNO, BCNO05, BCNO12, BCNO20 and BCNO 37.



The numerical simulation was performed using HFSS for validation of the samples as DRAs and to obtain the distant field parameters, such as gain, directivity, radiation efficiency, bandwidth, radiation diagram and Smith Chart. All the results obtained reveal that there is a small difference between the experimental and simulation results; this shows that the numerical simulation was effective. The real and imaginary impedances are shown in Fig. 8.

Figure 8: Simulated real and imaginary impedance of BCNO and BCNo-CTO.



The experimental and simulated data are in full agreement. Increasing the CTO concentration causes a shift in the peak frequency of the impedances. This numerical simulation profile is observed in all

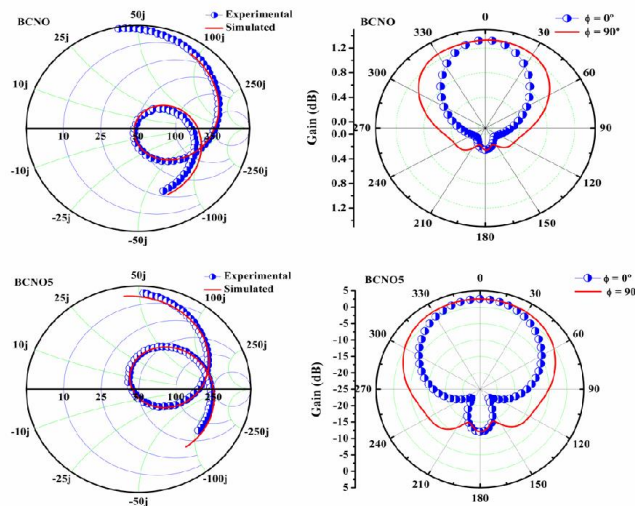
samples. Far-field parameters are shown in Table 5, which also presents gain, radiation efficiency, bandwidth, permittivity and loss tangent for all fabricated DRAs.

Table 5: Simulated data in HFSS and  $\tau_f$

Sample	$f_{Exp}$	$f_{Sim}$	Gain (dB)	$\epsilon_R$ (%)	$\epsilon'_{sim}$	BW <sub>Sim</sub> (MHz)	$\tau_f$ (ppm / °c)
BCNO	5.07	5.07	4.51	69.29	17.47	468.64	-330.45
BCNO05	4.33	4.32	4.24	64.71	16.06	360.05	-159.0
BCNO12	3.96	3.96	3.81	55.45	17.56	348.56	-148.9
BCNO20	3.88	3.88	4.39	65.24	18.10	278.90	-77.31
BCNO37	4.13	4.14	4.56	69.94	17.51	261.63	-0.98

The best values of gain and radiation efficiency were for the BCNO37 sample and the highest bandwidth was the BCNO sample, showing that BCNO and its compounds with CTO are suitable for use as DRAs. Figure 9 shows the radiation pattern of BCNO and BCNO05 obtained by numerical simulation. The profile of the radiation diagram is compatible with the profile of a cylindrical DRA, where we observe the maximum radiation at  $\theta = 0$  and  $\phi = 90^\circ$ .

Figure 9: Smith charge and radiation diagram of samples BCNO and BCNO05.



All other DRAs follow the same profile. The symmetry of the lobes indicates an effective coupling between the probe and the sample in the setup in Fig. 6. The Smith chart presented shows excellent concordance between the measured values and the simulated values, validating the study method. All samples presented the graph cross the real axis precisely at 50 Ohms, indicating a perfect impedance matching of line-antenna impedances.

## Conclusions

The addition of CTO into the BCNO ceramic matrix shows better thermal stability at around 37 wt%. The addition of CTO promotes a decrease in the density of the composites, allowing important applications in projects in which the weight is an important parameter for new device design. Nyquist diagrams were well fitted using two associations of R–CPE and the addition of CTO promoted an increase in the BCNO resistance due to the contribution of the grain and the boundary of the grain. The application of these composites as DRA was satisfactory since all the samples functioned as antenna and the reflection coefficient of the composites was below -10 dB, gains were above 3.81 dB and radiation efficiency was above 55.46%.

### Acknowledgements

The authors are grateful to CNPq (402045/2013-0), the US Air Force Office of Scientific Research (AFOSR) (FA9550-16-1-0127) and CNPq (Process: 402561/20074, Edital MCT/CNPq nº 10/2007) for providing financial support.

### References

- [1] A.J. Moulson, J.M. Herbert, *Electroceramics: Materials, Properties, Applications*, Wiley, 2003.
- [2] M.T. Sebastian, *Dielectric Materials for Wireless Communication*, Elsevier Science, Oxford, 2010. doi:<http://dx.doi.org/10.1016/B978-0-08-045330-9.00006-6>.
- [3] M. Ohring, *Engineering Materials Science*, United Kingdom, 1995.
- [4] K.M. Luk, K.W. Leung, *Dielectric Resonator Antennas*, Research Studies Press, Hertfordshire, 2003.
- [5] J. Intrater, A Review of: “ Sintering of Ceramics , M. N. Rahaman,” *Mater. Manuf. Process.* 23 (2007) 111–112. doi:[10.1080/10426910701623956](https://doi.org/10.1080/10426910701623956).
- [6] R.V.B. Campos, C.L. Bezerra, L.N.L. Oliveira, D.X. Gouveia, M.A.S. Silva, A.S.B. Sombra, A Study of the Dielectric Properties of Al<sub>2</sub>O<sub>3</sub>–TiO<sub>2</sub> Composite in the Microwave and RF Regions, *J. Electron. Mater.* 44 (2015) 4220–4226. doi:[10.1007/s11664-015-3958-3](https://doi.org/10.1007/s11664-015-3958-3).
- [7] G. Blasse, New compounds with perovskite-like structures, *J. Inorg. Nucl. Chem.* 27 (1965) 993–1003. doi:[10.1016/0022-1902\(65\)80409-2](https://doi.org/10.1016/0022-1902(65)80409-2).
- [8] T. NAGAI, W. ITO, T. SAKON, Relationship between cation substitution and stability of perovskite structure in SrCoO<sub>3</sub>– $\delta$ -based mixed conductors, *Solid State Ionics.* 177 (2007) 3433–3444. doi:[10.1016/j.ssi.2006.10.022](https://doi.org/10.1016/j.ssi.2006.10.022).
- [9] K. Yoshii, Magnetic Transition in the Perovskite Ba<sub>2</sub>CoNbO<sub>6</sub>, *J. Solid State Chem.* 151 (2000) 294–297. doi:[10.1006/jssc.2000.8656](https://doi.org/10.1006/jssc.2000.8656).

- [10] G. Wang, C. Wang, S. Huang, C. Lei, X. Sun, T. Li, L. Liu, Origin of Colossal Dielectric Behavior In Double Perovskite  $\text{Ba}_2\text{CoNbO}_6$ , *J. Am. Ceram. Soc.* 96 (2013) 2203–2210. doi:10.1111/jace.12318.
- [11] G.J. Wang, C.C. Wang, S.G. Huang, X.H. Sun, C.M. Lei, T. Li, L.N. Liu, Origin of the colossal dielectric properties in double-perovskite  $\text{Sr}_2\text{CoNbO}_6$ , *AIP Adv.* 3 (2013) 22109. doi:10.1063/1.4791763.
- [12] B.W. Hakki, P.D. Coleman, A Dielectric Resonator Method of Measuring Inductive Capacities in the Millimeter Range, *IEEE Trans. Microw. Theory Tech.* 8 (1960) 402–410. doi:10.1109/TMTT.1960.1124749.
- [13] M.A.S. Silva, T.S.M. Fernandes, A.S.B. Sombra, An alternative method for the measurement of the microwave temperature coefficient of resonant frequency ( $\tau_f$ ), *J. Appl. Phys.* 112 (2012) 74106. doi:10.1063/1.4755799.
- [14] H.M. Rietveld, A profile refinement method for nuclear and magnetic structures, *J. Appl. Crystallogr.* 2 (1969) 65–71. doi:10.1107/S0021889869006558.
- [15] S. Rajesh, K.P. Murali, R. Ratheesh, Preparation and characterization of high permittivity and low loss PTFE/ $\text{CaTiO}_3$  microwave laminates, *Polym. Compos.* 30 (2009) 1480–1485. doi:10.1002/pc.20716.
- [16] M.C. Romeu, R.G.M. Oliveira, A.J.M. Sales, P.M.O. Silva, J.M.S. Filho, M.M. Costa, A.S.B. Sombra, Impedance spectroscopy study of  $\text{TiO}_2$  addition on the ceramic matrix  $\text{Na}_2\text{Nb}_4\text{O}_{11}$ , *J. Mater. Sci. Mater. Electron.* 24 (2013) 4993–4999. doi:10.1007/s10854-013-1514-6.
- [17] D.V.M. Paiva, M.A.S. Silva, T.S. Ribeiro, I.F. Vasconcelos, A.S.B. Sombra, J.C. Góes, P.B.A. Fachine, Novel magnetic–dielectric composite ceramic obtained from  $\text{Y}_3\text{Fe}_5\text{O}_{12}$  and  $\text{CaTiO}_3$ , *J. Alloys Compd.* 644 (2015) 763–769. doi:10.1016/j.jallcom.2015.05.053.
- [18] X.-Z. Yuan, C. Song, H. Wang, J. Zhang, *Electrochemical Impedance Spectroscopy in PEM Fuel Cells*, Springer London, London, 2010. doi:10.1007/978-1-84882-846-9.
- [19] J.B. Huang, B. Yang, C.Y. Yu, G.F. Zhang, H. Xue, Z.X. Xiong, G. Viola, R. Donnan, H.X. Yan, M.J. Reece, Microwave and terahertz dielectric properties of  $\text{MgTiO}_3$ – $\text{CaTiO}_3$  ceramics, *Mater. Lett.* 138 (2015) 225–227. doi:10.1016/j.matlet.2014.09.122.
- [20] X. Zhang, J. Zhang, M. Wang, X. Zhang, H. Zhao, X.-J. Wang, Investigation on the improvement of red phosphorescence in  $\text{CaTiO}_3:\text{Pr}^{3+}$  nanoparticles, *J. Lumin.* 128 (2008) 818–820. doi:10.1016/j.jlumin.2007.12.010. [21] C.A. Balanis, *Antenna Theory: Analysis and Design*, Wiley, 2012.